

Hysteretic behaviour of steel fibre RC coupled shear walls under cyclic loads: Experimental study and modelling

Peer-reviewed author version

Zhao, Jun; CAI, Gaochuang; Si Larbi, Amir; Zhang, Yang; Dun, Huahua; DEGEE, Herve & VANDOREN, Bram (2018) Hysteretic behaviour of steel fibre RC coupled shear walls under cyclic loads: Experimental study and modelling. In: ENGINEERING STRUCTURES, 156, p. 92-104.

DOI: 10.1016/j.engstruct.2017.11.006

Handle: <http://hdl.handle.net/1942/25380>

1 Words: 8260; Number of figures: 13; Number of tables: 2

2 **Hysteretic behaviour of steel fibre RC coupled shear walls under**  
3 **cyclic loads: experimental study and modelling**

4

5 **Jun Zhao**, Dr. Eng.

6 School of Mechanics and Engineering Science, Zhengzhou University, Zhengzhou, China

7 **Gaochuang Cai\***, Ph.D.

8 Faculty of Science, Technology and Communication, University of Luxembourg, Luxembourg,

9 Luxembourg

10 Laboratoire de Tribologie et de Dynamique des Systèmes, Ecole Nationale d'Ingénieurs de Saint-

11 Etienne, University of Lyon, France

12 **Amir Si Larbi**, Ph.D.

13 Laboratoire de Tribologie et de Dynamique des Systèmes, Ecole Nationale d'Ingénieurs de Saint-

14 Etienne, University of Lyon, France

15 **Yang Zhang**, M. Eng., **Huahua Dun**, M.Eng.

16 School of Civil Engineering, Zhengzhou University, Zhengzhou, China

17 **Hervé Degée**, Ph.D., **Bram Vandoren**, Dr. Eng.

18 CERG, Faculty of Engineering Technology, Hasselt University, BE3500, Hasselt, Belgium

19

20 **\* Corresponding author:**

21 University of Luxembourg, Luxembourg, Luxembourg

22 Email: [gaochuang.cai@hotmail.com](mailto:gaochuang.cai@hotmail.com)

# 24 **Hysteretic behaviour of steel fibre RC coupled shear walls under cyclic** 25 **loads: experimental study and modelling**

26

27

## 28 **Abstract**

29 This paper presents the hysteretic behaviour of three 1/3-scale three-storey steel fibre reinforced  
30 concrete (SFRC) coupled shear walls (CSWs) under cyclic loads. The deformation, ductility, energy  
31 dissipation, stiffness and crack propagation of the specimens are also discussed and analysed. The  
32 results show steel fibre improves the ductility and energy dissipation capacity, and restrains the crack  
33 propagation of the CSWs, and delays the degradation of their lateral stiffness and force. Based on the  
34 experiments, a simple trilinear model is developed to simulate the skeleton curve of lateral force-  
35 displacement of the SFRC CSWs. Through analysing several typical cycles of the hysteretic of these  
36 CSWs, the feature points of the proposed hysteretic model are defined which subsequently is used to  
37 evaluate the complete hysteretic behaviour of the CSWs. Using existing experimental data and this  
38 study, several representative experimental hysteretic cycles are compared with the proposed model.  
39 The result indicates a good agreement is reached between the model and experimental results.

40

41 **Keywords:** Steel fibre reinforced concrete; Coupled shear wall; Skeleton curve; Hysteretic model;  
42 Seismic assessment;

43

## 44 **1. Introduction**

45 Reinforced concrete (RC) coupled shear walls (CSWs) are widely applied in high-rise and multi-  
46 storey building systems to provide an effective resistance to horizontal loads such as wind or seismic  
47 effects. Fig.1 shows the seismic effects and design method of RC coupled shear wall systems. With  
48 the demand of high-rise and multi-storey buildings, it is very significant and necessary to guarantee

49 that this kind of support elements in building structures can effectively withstand earthquakes without  
50 collapses or unreparable damages. In order to accomplish this goal, RC CSWs usually are designed to  
51 possess high lateral resistance strength, excellent deformation, high energy dissipation capacity and  
52 stable degradation of post-peak stiffness which all can provide a good control to the horizontal  
53 displacement or storey drift of the structures.

54

55 A number of experimental studies and numerical analyses have been conducted on RC CSWs in the  
56 past four decades (Paulay and Binney 1974; Chaallal and Ghlamallah 1996; Chaallal *et al.* 1996a;  
57 Kuang *et al.* 1999; Aksogan *et al.* 2003; Lu and Chen 2005). Based on these studies, several basic  
58 design rules, calculation methods, and analytic models had been established. The studies also had  
59 mentioned one important fact that the behaviour of coupling systems (mainly coupling beam) greatly  
60 affects the structural behaviour of the RC CSWs subjected to seismic effects. These coupling elements  
61 usually connect two shear walls in series to transfer the vertical force to get better-distributed load and  
62 meet the deformation demands of the structures. This is different with the ones in cantilever shear  
63 wall, in which the stiffness, strength, ductility, and dissipating energy of the entire structural system  
64 are wholly contingent on the response of the plastic hinge region of the structures. Therefore, the  
65 behaviour of coupling beams is very important to the behaviour of CSW system for the elements can  
66 distribute effectively the external load effects, rather concentrate the effects on the plastic hinge  
67 region of shear walls. However, RC beams is expected to possess stable hysteretic response under  
68 reversed loads, a sufficient confinement of concrete in coupling beam and an anchorage of the  
69 reinforcements in shear walls should be provided. This often leads to the fact that the coupling beams  
70 are designed as a deep beam with heavy reinforcements increasing construction cost and cast  
71 inconvenience. In order to improve the resistance behaviour of coupling beams (CBs), many types of  
72 CBs have been proposed such as steel CBs (Harries *et al.* 1993; Park and Yun 2005, 2006; Cheng *et*  
73 *al.* 2015), concrete-steel composite CBs (Gong and Shahrooz 2001; Harries *et al.* 2000), concrete

74 filled tube CBs (Hu *et al.* 2016), partially post-tensioned CBs (Barbachyn *et al.* 2016), fibre  
75 reinforced concrete CBs (Chaallal *et al.* 1996b; Parra-Montesinos 2005; Canbolat *et al.* 2005; Zhang  
76 *et al.* 2007; Cai *et al.* 2016).

77

78 To understand the basic behaviour of RC CSWs using conventional concrete under seismic loads,  
79 according to a short review of RC CSWs or RC CBs, several conclusions are drawn:

- 80 ○ The coupling beams in CSW systems have two main beneficial effects: (1) they can reduce the  
81 required moment of CSW system comparing with the one in two individual walls; (2) and they  
82 can effectively dissipate earthquake energy over the entire height of the walls (Aristizabal-  
83 Ocfaoa 1987).
- 84 ○ The three main types of the failure modes of ductile CSWs are: flexural failure of CB, shear  
85 failure of CB and rigid action of the CBs in the CSWs, depending on the degree of the  
86 interaction and resistance behaviour of the CBs in the system (Subedi 1989);
- 87 ○ The coupling beam at second floor of CSW structures usually yields first and stops resisting  
88 lateral deformation of the system;
- 89 ○ The use of diagonal reinforcements is an effective method to enhance the ductility and load  
90 resistance capacity of coupling beams. However, the addition of the reinforcement also brings  
91 new problems such as cast difficulty of concrete in beam-adjacent wall joint region;
- 92 ○ When CSW systems are subjected to large lateral deformation, most of the lateral force is  
93 resisted by the shear walls in the CSWs for the CBs have already undergone the effect of the  
94 inelastic deformation and usually failed at that moment;
- 95 ○ The applied axial load of CSWs has a significant influence on the lateral stiffness of the entire  
96 structure. Besides, in CSW system, the flexural deformation at the first floor is the highest and  
97 decreases along the height of CSW;
- 98 ○ The performance-based seismic designs have only begun to address in fibre reinforced concrete

99 structural walls. Just limited experimental investigations focused on the seismic response and  
100 damage assessment of the CSW systems to support the development of numerical analysis  
101 method, especially large-scale experimental study;

- 102 ○ According to past experimental and survey studies, when RC CBs have a small shear span  
103 ratio, their shear failure usually results in that the entire CSW system works as two independent  
104 individual shear walls. This affects significantly the behaviour of the entire CSW system in  
105 subsequent seismic loads.

106

107 In addition, according to existing experimental studies (Chaallal *et al.* 1996b; Parra-Montesinos 2005;  
108 Zhang *et al.* 2007; Canbolat *et al.* 2005; Zhao and Dun 2014), the use of steel fibre (SF) in RC CBs or  
109 RC shear walls improves the stiffness, ductility and energy dissipation capacity of these members and  
110 enhances their seismic and cracking resistance behaviours as well. However, these studies have just  
111 focused on the effect of steel fibre on individual RC coupling beams or cantilever shear walls such as  
112 the ones reported by our research group (e.g. Zhao and Dun 2014; Zhang 2007). Only a few studies  
113 (Lequesne *et al.* 2011, 2012; Parra-Montesinos *et al.* 2017) are available which concerned the  
114 application of fibre in RC CSWs such as the RC shear walls coupled by fibre reinforced concrete  
115 (SFRC) CBs (Lequesne *et al.* 2011; 2012, Meng 2013) or SFRC CBs (Cai *et al.* 2016). The research  
116 results illustrated that the use of steel fibre improved the entire deformation and lateral resistance of  
117 the RC CSWs subjected to seismic effects by enhancing the shear resistance, stiffness, energy  
118 dissipation and ductility of CBs. The beams without diagonal steel reinforcements also solve the  
119 congestion of steel rebars in the joint region of the CSW system (Cai *et al.* 2016). The clear  
120 understanding of the entire behaviour of RC SCWs mainly including co-workability and coupling  
121 effectiveness between RC CBs and shear walls is very significant to their design and application with  
122 the considerations of seismic effects. As a consequence, in order to develop the design methods of  
123 SFRC CSWs and support the development of the performance-based design of CSWs, more

124 experimental data and analysis models of CSWs are expected.

125 The main objectives of the current research are to investigate experimentally the seismic hysteretic  
126 behaviour of coupled SFRC-CSWs (SFSWs) and to model the skeleton and hysteretic curve of the  
127 coupled SFSWs for providing valuable recommendations to their seismic design. To be specific, this  
128 paper emphasizes to (a) study the failure modes of SFSWs, deformation and resisting mechanism of  
129 various elements of the SFSWs, (b) analyse the ductility, stiffness, and energy dissipation behaviour  
130 of the SFSWs, and (c) model the skeleton and hysteretic curves of the elements.

131

## 132 **2. Research significance**

133 The study of the application of steel fibres in RC CSWs, one kind of the important support elements  
134 in modern earthquake resistance structure systems, is very significant to develop the seismic design  
135 method and promote the application of the structures. Unfortunately, just a few studies have been  
136 reported focusing on steel fibre RC CSW system. In this study, the seismic response and resistant  
137 mechanism of three coupled SFRC-CSWs are experimentally investigated. The skeleton curve and  
138 hysteretic behaviour of the specimens are discussed and modelled respectively. Additionally, several  
139 key recommendations will be provided to improve the design of CSW system and to propel the  
140 establishment of relevant codes for them in the future.

141

## 142 **3. Experimental investigation**

### 143 **Test specimens**

144 The experimental program in this study consists of three approximate 1/3-scale three-storey planar  
145 RC/SFRC CSWs designed per the Chinese technical specification for the concrete structures of tall  
146 buildings JGJ3-2010 (2010), the Chinese code CECS38:2004 (CEC 2004), and the National testing  
147 method guideline JGJ101-1996 (CIS 1996). Each CSW specimen has a 3750mm total height and a  
148 1900mm total wall length and includes several wall pieces with 100mm of thickness. The length of

149 the walls of the CSW system is 600mm with an RC edge column having a width of 400mm and height  
150 of 100mm. The sectional size of the coupling beams in each CSW specimen is 500 x 250mm (length x  
151 depth) with a span-to-depth ratio of 2.0. In order to avoid the congestion of steel reinforcements, in  
152 particular in the zone of the beam-column joints, no diagonal steel reinforcement was used in all  
153 coupling beams of the CSW specimens. Fig.2 shows the details of the CSW specimens such as the  
154 dimension of various elements and reinforcement arrangement. According to the previous experience  
155 in practical engineering and existing literature (Song and Hwang 2004; Singh *et al.* 2014; Yu *et al.*  
156 2014; Borg *et al.* 2016), the usually-used volume fraction of steel fibre in concrete ranges from 0.5%  
157 to 2.0%. Tejchman and Kozicki (2010) also reported that the crack load and ultimate load were found  
158 to increase with the volume fraction of fibre in concrete. Therefore, the study use two typical volume  
159 fractions of steel fibre (1% and 2%) in the specimens. Table.1 lists the details of the main parameters  
160 of the test specimens, while their main features are summarized as follow,

- 161 (a) Specimen SFSW-1—using conventional concrete, as reference specimen;
- 162 (b) Specimen SFSW-2—using concrete with 1% steel fibre (volume fraction), same  
163 reinforcement arrangement as the SFSW-1;
- 164 (c) Specimen SFSW-3—using concrete with 2% steel fibre (volume fraction), same  
165 reinforcement arrangement as the SFSW-1;

166

167 On the other hand, uniformly distributed longitudinal and transverse steel reinforcements were  
168 allocated taking into account the flexural and shear resistance of these elements. The reinforcement  
169 arrangements of the CSWs were followed the Chinese code CECS38:2004 (CEC 2004) and the  
170 Standard of tall building JGJ3-2010 (CIS 2010). According to the study conducted by Harries (2001),  
171 the coupling degree of all CSW specimens are less than 55%. The overall ratios of longitudinal and  
172 transverse reinforcements of the shear walls of the three CSW specimens are same, 1.26% and 1.15%  
173 respectively. The details of the reinforcements of the coupling beams, base beams and shear walls of



174 the CSWs are shown in Fig.2. The area ratios of the longitudinal and transverse steel rebars of the  
175 CBs of the CSW specimens are 1.25% and 0.3%, respectively. Besides, a special earthquake report  
176 (EERI 2010) indicated that relatively high levels of axial stress likely led to the great damage suffered  
177 by buildings. However, quite few research (Zhang and Wang 2000; Su *et al.* 2007) has been reported  
178 about the seismic behaviour of shear walls or CSWs, especially SFRC CSWs. With the increase in the  
179 axial load ratio, the height of concrete spalling rises (Jiang *et al.* 2013). As a start of the experimental  
180 research program of SFRC CSWs and referring to the previous studies (Kabeyasawa and Hiraishi  
181 1998; Gupta and Rangan 1998; Yun *et al.* 2004; Farvashany *et al.* 2008; Deng *et al.* 2008; Jiang *et al.*  
182 2013), a low vertical axial load ( $0.1f_{c}A_{g}$ ) was used in this study.

183

#### 184 **Material properties**

185 The compressive strength of used concrete was 40MPa, which was transferred to a mean measure  
186 strength (41.70MPa) of standard cubic ( $150\times 150\times 150\text{ mm}^3$ ) specimens per the test standard of CECS  
187 13-2009 (CIS 2009). The same concrete with different volume fractions of steel fibre were applied in  
188 the SFSW-2 and SFSW-3 which have a measured cubic compressive strength of 46.44MPa and  
189 50.4MPa, respectively. To avoid the lumping of steel fibre in concrete, steel fibre was first mixed with  
190 coarse aggregates and then mixed slowly with a dry combined mix consisting of cement and fine  
191 aggregates. Once all of the dry mixes have been stirred uniformly, water was then added to make the  
192 steel fibre concretes. Two different types of reinforcing rebars were used in the specimens: plain steel  
193 rebars (HPB 300,  $\phi 6$ ,  $\phi 8$  and  $\phi 10$ ) were used for shear walls and coupling beams, and deformed steel  
194 rebars (HRB 400,  $\phi 14$  and  $\phi 20$ ) were applied for the base beams. The details of Young's modulus,  
195 yielding and ultimate strengths of the steel rebars were obtained through relevant Chinese standard  
196 tests. The used steel fibre is a kind of corrugated steel fibres which has an equivalent diameter of  
197 0.76mm, a length of 32mm and a yielding strength of 380MPa provided by the manufacturer,  
198 respectively.

199

## 200 **Instrumentations and testing procedure**

201 The test setup used in this study is shown in Fig.3. Each of specimens was mounted on a strong floor.  
202 **A low vertical load** ( $0.1f_{fc}A_g$ , about 340kN) was first applied through a combined loading system  
203 consisting of four hydraulic vertical jacks, which can move horizontally with the top of the specimens,  
204 as the Parts 2-4 shown in Fig.3. A lateral reverse load was then applied to the top beam of the CSW  
205 specimens by a horizontal hydraulic jack fixed on a strong reaction wall, as the Part 1 shown in Fig.3.  
206 The reinforcing rebars of the specimens were equipped with several electrical strain gauges to  
207 measure their strains, and the deformation of the specimens was monitored by a few Linear Variable  
208 Differential Transformers (LVDTs). In the reinforcing rebars of the edge RC columns of the CSWs,  
209 30 strain gauges were used to monitor their strain.

210

211 A quasi-static cyclic loading was used at each of specimens and divided clearly into two stages. To  
212 observe the crack propagation of each specimen at early stage, a force-control loading (single cyclic  
213 for each level) was applied first until the yielding of certain longitudinal reinforcement was observed  
214 or when the envelop curve of the force-displacement of the specimen presents an obvious **yielding**  
215 **point**. At this moment, entire CSW specimen was considered to reach its yielding displacement ( $\Delta_y$ ).  
216 Subsequently, to simulate the impacts of earthquake, a series of displacement-control loading cycles  
217 (2 cycles for each target level) were applied to each specimen, starting after the specimen reached its  
218 yielding displacement ( $\Delta_y$ ) and increasing with  $0.5\Delta_y$  (i.e.  $1.5\Delta_y$ ,  $2.0\Delta_y$ ,  $2.5\Delta_y$ ,  $3.0\Delta_y$ ,  $3.5\Delta_y$ ,  $4.0\Delta_y$ ).  
219 During the tests, the crack propagation, damage, deformation and lateral force-development of these  
220 specimens were recorded and monitored. For the security of test people and equipment, the test is  
221 finished if the lateral force of the specimens reduces to 85% of the maximum measured force or the  
222 lateral displacement of the specimen reaches about 4 times yielding displacement ( $4.0\Delta_y$ ).

223

## 224 4. Test results and analysis

### 225 4.1 General behaviour

226 The main experimental results about the hysteretic behaviour of the specimens are presented in Fig.4.

227 The reference specimen SFSW-1 elastically resists its lateral deformation at the initial stage until the

228 lateral force ( $F$ ) reaches 50kN. At this moment, the first lateral flexural crack was observed on the end

229 of the two walls at the first floor in push loading direction. At the same time, several vertical cracks

230 were confirmed at the ends of CBs in push and pull directions (500-600mm from the ends). The first

231 shear crack was found in the shear walls at the place of 30-150mm from the bottom ends of the first

232 floor shear walls when the lateral load was 125kN (average level in two directions). From  $1.0\Delta_y$  to

233  $3.0\Delta_y$ , the cracks mentioned above developed quickly while a few new cracks appeared, and the

234 concretes at the hinge zones of the CBs and the ends of shear walls were crushed. When the lateral

235 displacement of the reference CSW reached  $2.0\Delta_y$ , the specimen presented its maximum strength.

236 When the lateral displacement of the specimen was  $4.0\Delta_y$ , although no new crack was observed, more

237 concretes crushing between CBs and shear walls were found or the exposure of some longitudinal

238 steel rebars was confirmed. This severely crushed concrete so that the entire cross-section of the

239 specimen was cut through leading to its structural failure. Like vertical support members such as RC

240 columns, the reverse lateral loading cycles make the RC CSW show an obvious degradation in the

241 lateral resistance force at the later stage.

242

243 In the SFRC CSW specimens, similar experimental observations were found in both two specimens at

244 the initial stage, except for the crack propagation of shear walls is slow. The use of SFRC delays the

245 propagation of the flexural and shear cracks in the shear walls and shear-cracks in the coupling beams

246 (see Fig.5). At the same time, the use of steel fibre makes the shear walls get a more uniform stress

247 distribution to resist the external loads uniformly. However, SFRC did not bring an obvious

248 improvement in the resistance of flexural cracks of the coupling beams in the specimens. Besides,

249 similar damages as the ones in the reference CSW were found in the two SFRC CSWs such as  
250 concrete crushing. With regards to the enhancement of CBs caused by the addition of steel fibre, the  
251 resistance of shear walls in the SFRC CSWs was higher than the one in the reference RC CSW, which  
252 resulted in that the longitudinal steel rebars of the specimens fractured when their lateral displacement  
253 was  $4.0\Delta_y$ .

254

255 In the term of hysteretic behaviour, comparing with the reference RC CSW specimen, the SFRC CSW  
256 specimens present a plumper hysteretic behaviour with a higher lateral stiffness and stronger bearing  
257 capacity and more stable degradation of lateral force at the post-peak stage. In order to understand  
258 clearly the crack propagation of the SFRC CSWs, their load cycles were divided into three main  
259 stages shown in Fig.4. (1) At the early stage of the loading, most of cracks centred and developed  
260 quickly at the ends of CBs because of the large deformation caused by a strong bending moment at  
261 the top of shear walls. This fits well with the design of these specimens in this study. In the SFRC  
262 CSWs, however, the use of steel fibre makes these CBs present a relative slower crack propagation.  
263 (2) At middle stage of the loading, many lateral flexural cracks propagated in the two shear walls of  
264 the SFRC CSWs. However, the reference RC CSW resisted the propagation of the cracks through the  
265 action of longitudinal reinforcements until the cracks occurred in the upper part of shear wall. But  
266 steel fibre improved the cracking resistance of the shear walls making the entire CSW present more  
267 uniform stress situation. (3) After the coupling beams of CSWs stopped working due to more and  
268 wider interfacial cut-through cracks, the crack propagation of the entire CSWs focused on the ends of  
269 the shear walls. The cracks widened sharply at the below end of the wall leading to more concrete  
270 crushing. A few flexural-shear cracks occurred at the shear walls at each floor meaning the steel fibre  
271 provided a good restriction to the horizontal flexural cracks.

272

273 The failure of all specimens were flexural-dominate failure model. This indicates the design of the

274 CSWs per the Chinese code JGJ 3-2010 (CIS 2010) is acceptable. The use of steel fibre has a  
275 significant influence on the crack propagation and deformation of the CSW specimens, including  
276 control of the number of crack and uniformly distribution of these cracks. Besides, the crushing of  
277 concrete at the joint zone between shear walls and CBs was lightened, as shown in Fig.5.

278

#### 279 ***4.2 Deformation mechanism of RC/SFRC CSWs***

##### 280 (1) Deformation of shear walls

281 The deformation situation of shear wall is helpful to understand the transfer mechanism of external  
282 loads in CSW system. As shown in Fig.6, main experimental observations were drawn as,

283 a. The longitudinal reinforcements located at the critical sections such as the ends of shear walls  
284 presented their highest strain levels in all tested CSW specimens.

285 b. According to the test results, the deformation of the reinforcements at the ends of the RC CSW  
286 present a considerable elastic feature, even when the lateral resistance force of the CSW  
287 decreases at the later stage. This is explained by the fact that the entire CSW system can be  
288 switched into two single shear walls after the CBs stopped working at large deformation stage.  
289 When steel fibre was used in RC CSWs, the lateral resistance and deformation of CBs were  
290 improved enhancing the lateral deformation capacity of the entire CSW system.

291 c. The use of steel fibre makes the CSW system obtain a more uniform stress distribution by  
292 controlling the deformation and damage of the end zones of shear walls and transferring the  
293 stress to the reinforcements of the walls at above floors. This was verified by the fact that the  
294 strain of longitudinal reinforcements in the RC CSW was smaller than the one in SFRC-CSWs  
295 at the second and third floor.

296 d. Because of the additional confinement effect of the top RC columns on the third floor of SFRC  
297 CSWs, the strain of reinforcements at the third floor is usually higher than the one at the

298 second floor. However, these reinforcements still did not reach their yielding strengths. It  
299 should be noted that the top loading beam also serves to restrain axial forces in the beams and  
300 improve the behaviour of entire CSW for it was cast integrally with the shear walls. For this, all  
301 specimens exhibit a classic single large crack appearing at the ends of the beams. Similar to the  
302 results reported by Paulay (1971), this leads to sliding shear failures, particularly where tensile  
303 forces are developed in the beams.

304 e. After some longitudinal reinforcements of the shear walls in SFRC CSWs reach their ultimate  
305 strengths, for the walls still needed to resist the lateral deformation, the strains of the  
306 reinforcements in the upper floors increased (see Fig.6).

307

308 (2) Deformation of coupling beams in CSWs

309 The strains of the reinforcements of the CBs in the reference RC CSW are usually less than the ones  
310 in SFRC CSWs. It is attributed to that the large crushed concrete cover in RC coupling beams makes  
311 the beams to stop providing an effective coupling action for the deformation of the two shear walls. In  
312 the SFRC CSWs, however, the use of steel fibre improves the coupling action of CBs which makes  
313 the strains of the reinforcements in these SFRC CSWs obtain a continuous increase.

314 Based on above analysis, it was found that steel fibres can effectively enhance the shear resistance of  
315 CBs which enhances the deformability of the entire CSW system, and can reduce the concrete  
316 crushing in the hinge zones of the CBs which ensures their coupling action at later stage. These make  
317 the CBs in SFRC CSWs more effective to resist the reverse seismic loads of the entire behaviour of  
318 the structure. This is also helpful to control the degradation of lateral stiffness and to improve the  
319 lateral resistance force, energy dissipation of the CSW systems.

320

321 ***4.3 Seismic response—Ductility, stiffness and energy dissipation***

322 Ductility, stiffness and energy dissipation capacity are important assessment indexes to evaluate the  
323 seismic response of RC structural members. A high level of ductility means RC members have a  
324 stable deformation without a rapid and substantial reduction in the lateral strength of the RC members  
325 subjected to strong earthquake (e.g. after drift ratio of 1/50). Lateral stiffness is to evaluate the  
326 capacity of RC members resisting to their lateral deformation and to conduct an effective analysis of  
327 the global behaviour of RC structures. In addition, energy dissipation capacity reflects the ability of  
328 RC elements to absorb the earthquake energy caused by underground vibration, which usually  
329 dissipate the energy through the inelastic damage of the members or some additional damping  
330 devices. Referring to Fig.7, the detailed definition and description of the above indexes are  
331 summarized as below.

### 332 (1) Initial stiffness

333 The initial stiffness indexes discussed in this paper include initial elastic deformation stiffness  $K_{int}$  and  
334 nominal initial stiffness  $K_y$  (yielding stiffness) shown in Fig.7. As reported by Paulay and Priestley  
335 (1992), the quantity of the stiffness indexes related to lateral loads to ensure structural deformations.  
336 The two stiffness indexes are calculated secant displacement stiffness when the lateral displacements  
337 are 0.33 and 1.0 times the measured yielding displacement ( $\Delta_y$ ) of the member, respectively. In this  
338 study, the yielding displacement  $\Delta_y$  is a measured value of the lateral displacement obtained from the  
339 skeleton curve of load-displacement of the elements when an obvious inflection point (yielding point)  
340 of the skeleton curve occurs or when certain longitudinal reinforcement in the shear walls yields.

### 341 (2) Ductility indexes

342 Based on the previous studies, several methods to define the ductility of RC members have been  
343 proposed, including displacement and curvature ductility. For instance, energy method, 0.75 (Ghee *et*  
344 *al.* 1989) or 0.85-time ultimate lateral force, and equal-area method. In this study, referring to the  
345 research results reported by Ghee *et al.* (1989) and through measured yielding displacement ( $\Delta_y$ ),  
346 maximum lateral displacement ( $\Delta_{max}$ ) and ultimate displacement ( $\Delta_u$ ) corresponding to  $85\%V_{max}$

347 (Paulay and Priestley 1992; Pam *et al.* 2001; Memon and Sheikh 2005; Osorio *et al.* 2014), the  
 348 maximum and ultimate ductility indexes are defined as,

$$349 \quad \mu_{\max} = \frac{\Delta_{\max}}{\Delta_y} \quad (1)$$

$$350 \quad \mu_u = \frac{\Delta_u}{\Delta_y} \quad (2)$$

### 351 (3) Inter-storey drift ratio

352 The ultimate inter-storey drift ratio  $\delta_u$  is one of the important parameters to evaluate the deformation  
 353 capacity of RC elements and in relation to the height of the elements. It is expressed as,

$$354 \quad \delta_u = \frac{\Delta_u}{H} (\%) \quad (3)$$

### 355 (4) Total dissipated energy

356 Energy dissipation is a fundamental structural property of RC elements when subjected to seismic  
 357 demands. Energy dissipated of certain completed load cycle ( $i^{\text{th}}$  loop) ( $E_i$ ) is calculated by the area of  
 358 load-displacement curve encircled by this cycle, shown as the hatched area in Fig.7. The total  
 359 dissipated energy of RC members is a sum of all cycles of the loading until the lateral force of the  
 360 member reduce to 85%  $V_{\max}$ , is given by,

$$361 \quad E_T = \sum_{i=1}^n E_i \quad (4)$$

### 362 (5) Total work index $I_{wo}$

363 To evaluate the serviceability of RC elements subjected to a given loading history, Gosain *et al.*  
 364 (1977) propose a total work index  $I_{wo}$  which is expressed as,

$$365 \quad I_{wo} = \frac{1}{V_{\max} \Delta_y} \sum_{i=1}^n V_{i,\max} \Delta_{i,\max} \quad (5)$$

### 366 (6) Energy index $I_E$

367 Ehsani and Wight (1990) suggested a damage index  $I_E$  to evaluate the damage degree of RC elements  
 368 subjected to a given load history which is given by



$$I_E = \frac{1}{V_{\max} \Delta_y} \sum_{i=1}^n E_i \left( \frac{K_{\text{int}}}{K_y} \right) \left( \frac{\Delta_{i,\max}}{\Delta_y} \right)^2 \quad (6)$$

370

371 Table.2 gives a summary of the results of all above-mentioned indexes of the tested CSW specimens.

372 It was found that the use of steel fibre improved the initial stiffness, ultimate ductility, and energy

373 dissipation and working properties of the CSWs. This is attributed to two aspects, i.e. steel fibre

374 restricts the crack propagation of concrete at the ends of shear walls at early stage and reduces the

375 degradation of lateral resistance force at later stage. To be specific, the main benefits of steel fibre in

376 RC CSW are,

377 (a) SFSWs have a higher initial stiffness of about 1.4 times the one of RC CSW for the bridging

378 effect of the steel fibre in the concrete (Yap *et al.* 2016; Bharti *et al.* 2017);

379 (b) Steel fibre has a positive influence on the maximum lateral resistance capacity of RC CSWs

380 which indicates the shear resistance of SFSWs is partly from the shear contribution of SFRC

381 of coupling beams before they stop their coupling action;

382 (c) The maximum ductility levels ( $\mu_{\max}$ ) of the two SFRC CSWs are 1.06 and 1.38 times the one

383 of RC CSW when the volume fractions of steel fibre in concrete are 1% and 2% respectively;

384 (d) When the used volume fraction of steel fibres is 1%, though steel fibre did not enhance the

385 yielding displacement and inter-storey deformation capacity of the CSW, the ultimate

386 ductility of this specimen is 1.05 times one of RC CSW and their energy dissipation capacity,

387 energy index and total work index increased in 40%-60% comparing with the ones of the

388 reference specimen.

389

### 390 (7) Lateral secant stiffness vs. displacement

391 It is significant to RC structures to understand the degradation of lateral stiffness of RC members

392 under cyclic loads. Fig.8 shows the development of the lateral secant stiffness of all tested CSWs with

393 their lateral displacement. Because steel fibre resists the cracking of concrete located at the ends of  
394 shear walls due to its **bridging effect**, the lateral secant stiffness of SFRC CSWs is higher than the one  
395 in normal concrete at early stage. However, the degradation degree of the lateral stiffness of all CSWs  
396 increases sharply before the lateral displacement of the members reaches their yielding displacement  
397  $\Delta_y$ . Experimental observations verified that the deformation of the entire CSW was resisted by  
398 developing the flexural cracks at the ends of shear walls and the shear cracks on the shear walls at the  
399 second and third floor. At the later stage, the changing amplitude of the lateral stiffness of all  
400 specimens is quite gentle. This was explained by the facts that just a few new cracks were found in the  
401 CSWs at this stage and steel fibres stop their effective resistance to wide opened cracks.

402

## 403 **4 Analysis and modelling of skeleton curve and hysteretic loop**

### 404 **5.1 Modelling of skeleton curve of SFSWs**

405 In order to model the skeleton curve of the hysteretic behaviour of the RC members subjected to  
406 cyclic loads, the most widely-applied restoring force model is tri-linear restoring force model shown  
407 in Fig.9. The line 1 plotted in this figure presents three main feature points of the modelling curve of  
408 normal RC elements, i.e. cracking, yielding and maximum strength points respectively. For normal  
409 RC members, the yielding point could be quite different among different kinds of structural members  
410 due to the reduction of lateral stiffness after cracking. In well-designed SFRC elements, however, the  
411 lateral resistance of members after ultimate strength is still considerable and decreases slightly with  
412 the displacement as Line 2 shown in Fig.9. The experimental results of the study show the lateral  
413 stiffness of RC CSWs usually varies before they reach their maximum lateral force and the total  
414 degradation of the stiffness cannot be ignored. Therefore, a simplified tri-linear model based on FRC  
415 beam/columns model was suggested as Line 3 shown in Fig.9.

416

#### 417 *5.1.1 Definition of yielding point*

418 Generally, it was considered that the yielding point of RC members is reached when certain  
 419 longitudinal reinforcement yields or when the lateral force of the elements reaches 75-85% of their  
 420 maximum (ideal calculated or measured) strength (e.g. Ghee *et al.* 1989; Bayrak and Sheikh 1997).  
 421 However, in CSW systems, although SFRC coupling beam can provide a good coupling effect for its  
 422 high performance, the integrity of the systems is weak and significantly affects the lateral stiffness of  
 423 the entire member. This then influences the yielding of the CSW members. Referring to the research,  
 424 it is suggested that the lateral force of CSWs usually reaches 65% of their maximum strength when  
 425 the members yield in this study. Therefore, the yielding strength of SFSWs is calculated as,

$$426 \quad F_y = \alpha_1 F_u = 0.65 F_u \quad (7)$$

$$427 \quad K_y = \beta_y K_{int} \quad (8)$$

428 As described previously, the lateral stiffness of SFSWs has no very obvious changes before cracking  
 429 of the members, which is considered as a reduced initial stiffness  $K_{int}$ . Therefore, the yielding stiffness  
 430 of SFRW is expressed as Eq. (8). Regarding the reduction ratio of the initial stiffness of single SFRC  
 431 shear wall at the yielding situation, Zhao and Dun (2014) reported that it could be taken as 0.29 for  
 432 predicting the yielding stiffness. In this paper,  $K_{int}$  is calculated on the basis of the Chinese standard  
 433 JGJ3-2010 (CIS 2010) and given by,

$$434 \quad K_{int} = \frac{3E_c I_{eq}}{H^3} = \frac{1}{H^3} \frac{3E_c I_w}{1 + \frac{9\mu I_w}{A_w H^2}} \quad (9)$$

435 In SFRC CSWs, however, SFRC coupling beams improve the whole behaviour of the member which  
 436 then affects the development of lateral stiffness at this stage. Then, this positive effect of steel fibre  
 437 decreases greatly if the capacity of RC coupling beam is higher than the one of shear walls. This is  
 438 attributed to that the moment distribution and corresponding deformations of the various parts of  
 439 CSWs significantly are dependent on their stiffness level. The results of the present research already  
 440 verified the above analysis and present that the values of the reduction ratios of SFSW1-3 are 0.14,

441 0.19 and 0.16, respectively. Therefore, the change of lateral stiffness of SFSWs is affected by three  
 442 parts, i.e. the nonlinear behaviour of steel rebar and SFRC, and the reduction in the confinement of  
 443 coupling beams. With the above considerations, when the volume fraction of steel fibre in SFSWs  
 444 ranges from 1% to 2%, the simplified stiffness reduction ratio  $\beta_y$  is suggested to take as 0.2.

445

#### 446 5.1.2 Definition of maximum strength point— $M_{max}$ and $K_{max}$

447 As described previously, a well-design RC CSW system works similarly to a single RC shear wall  
 448 before reaching their maximum resistance status. Therefore, RC CSW is considered as an I-type RC  
 449 elements with openings same as reported by Zhao and Dun (2014). The design also should consider  
 450 the coupling effect of coupling beam and the resistance of the shear walls. Considering the positive  
 451 effect of RC edge columns and steel fibre on the entire behaviour of CSWs, a simplified calculation  
 452 model to predict the moment capacity of SFSWs  $M_{max}$  consisting of the moment resistance  
 453 compositions from transverse reinforcement ( $M_{st}$ ), longitudinal steel of RC edge columns ( $M_{sl}$ ),  
 454 enhancement effect of axial load ( $M_a$ ) and SFRC ( $M_{FRC}$ ) and is expressed as,

$$455 \quad M_{max} = M_{st} + M_{sl} + M_a + M_{FRC} \quad (10)$$

456 **In this equation, based on a detailed sectional analysis of RC/SFRC CSWs, the compositions provided**  
 457 **by the parts of the CSWs are summarized in Eqs. (11) to (14).**

$$458 \quad M_{st} = \frac{A_{sw} f_{yw}}{2h_{wo}} (h_w - h_b - 1.5x)(h_w - h_b + 0.5x) \quad (11)$$

$$459 \quad M_{sl} = f_y A_s (h_w - h_b) \quad (12)$$

$$460 \quad M_a = \frac{1}{2} N (h_{wo} - h_b) \quad (13)$$

$$461 \quad M_{FRC} = f_{fb} b_w x_t \left( h_w - \frac{x_t}{2} - \frac{x}{2} \right) \quad (14)$$

462 where, the concrete compressive strength of SFRC is calculated by the model proposed by Zhang  
 463 (2007) and detailed information is reached in the research reported by Zhao and Dun (2014). Through  
 464 the maximum moment of RC CSWs, the maximum lateral resistance force  $F_{max}$  is obtained.

465 On the other hand, with the considerations of the entire resistance of CSWs is less than a single shear  
466 wall with the same conditions (cross-section, reinforcements and concrete etc.), a reduction factor is  
467 introduced to modify the maximum moment  $M_{max}$  of the CSWs based on the original calculation of  
468 the two signal shear walls. To simplify the calculation procedure, the reduction factor is suggested as  
469 0.95 for the reference RC CSWs. Due to steel fibres improved the entire lateral resistance of RC CSW  
470 system, the reduction factor is taken as 0.9 for the SFRC CSWs in this study. About the lateral  
471 stiffness from yielding point to maximum strength point ( $K_{max}$ ), as presented previously, the lateral  
472 stiffness  $K_{max}$  of CSWs is assumed as 0.3 times initial stiffness,  $0.3K_{int}$ , referring to the experimental  
473 results in this study.

474

475 5.1.3 Definition of post-peak point of skeleton curve —  $F_u$  and  $K_u$

476 **Ultimate strength  $F_u$** — A number of researchers suggested the ultimate strength of RC elements (e.g.  
477 columns) was taken as 80%-90% of their maximum strength (Bayrak and Sheikh 1997). In this study,  
478 the ultimate strengths of SFRC CSWs were considered as 85% of the maximum strength, i.e.  $0.85F_{max}$   
479 (Hwang *et al.* 2005; Zhao and Dun 2014).

480 **Lateral stiffness at post-peak  $K_u$** — Due to the post-peak behaviour of RC CSWs is improved by steel  
481 fibre, the reduction of lateral stiffnesses of SFSWs should be slower than the one in normal CSW at  
482 this stage. Additionally, owing to coupling beams stop providing lateral resistance at the large  
483 deformation stage, the main influence factors of the stiffness are fibre concrete compressive strength  
484 and the volume fraction of steel fibre. In this paper, the lateral stiffness at post-peak was calculated as  
485 an equivalent stiffness multiplying an affecting ratio  $\beta_{wu}$  to the initial stiffness  $K_{int}$ . In each individual  
486 shear wall in CSW system, Zhao and Dun (2014) indicated the affecting ratio could be near to -0.02  
487 for SFRC shear walls. Therefore, with the consideration of the weak structural integrity of the CSW  
488 system but the good coupling action of SFRC coupling beams in SFSWs,  $\beta_{wu}$  is taken as 60~70% of  
489 the one of sign SFRC shear wall, i.e.  $K_u$  is -0.013 times of the initial stiffness  $K_{int}$ .

#### 490 5.1.4 Complete skeleton model

491 Based on the above analyses, the complete skeleton model curve of SFSWs (the volume fraction of  
492 steel fibre: 1%-2%) is expressed as,

$$493 \quad F = \begin{cases} K_y \Delta_x = \beta_y K_{int} \Delta_x & 0 \leq \Delta_x \leq \Delta_y \\ K_y \Delta_x + 0.03 K_{int} (\Delta_x - \Delta_y) & -\Delta_{max} \leq \Delta_x \leq -\Delta_y \text{ and } \Delta_y \leq \Delta_x \leq \Delta_{max} \\ K_y \Delta_x - 0.013 K_{int} (\Delta_x - \Delta_u) & -\Delta_u \leq \Delta_x \leq -\Delta_{max} \text{ and } \Delta_{max} \leq \Delta_x \leq \Delta_u \end{cases} \quad (15)$$

#### 494 5.1.5 Experimental verification of proposed model

495 To check the proposed model curve, some new research results (Meng 2013) were used. As shown in  
496 Fig.10, the calculated skeleton curves present a good agreement with the experimental curves which  
497 illustrate the proposed model can be used to predict the skeleton curve of the load-displacement of the  
498 SFSWs subjected to seismic loads.

499

## 500 5.2 Modelling of hysteretic curve of RC/FRC CSWs

### 501 5.2.1 Calibration of the rule for hysteretic curve

#### 502 (a) Before yielding of CSW members

503 Taking specimen SFSW-1 as an example shown in Fig.11 (a), according to the experimental results of  
504 the current study, the non-elastic deformation of CSW is slight before it reaches its yielding status. It  
505 means the plastic dissipated energy of the member could be ignored. Therefore, in this paper, the rule  
506 of the hysteretic curve before the yielding of the member is simply considered as a linear uploading or  
507 unloading cycle.

#### 508 (b) From yielding point to maximum strength point

509 Before CSW reaches its maximum strength or coupling beams stop providing deformation resistance,  
510 the restoring force rules of SFSW are same or similar as the ones of signal coupling beam/shear wall.  
511 Therefore, referring to the research results reported by Zhao and Dun (2014) and the experimental  
512 result in the current study shown in Fig.11 (b), a simplified restoring force model of SFSW are

513 obtained shown in Fig.12, including some key feature points (Points 1-8). The definition of the points  
514 is concluded as the following sections.

515 (1) Fixed feature points 1 and 5

516 As shown in Fig.12, each of hysteretic loops of the load-displacement curve has two key fixed points  
517 on its uploading and unloading branch, respectively. The lateral forces corresponding to the two  
518 points both are 0.3 times of yielding strength at the both directions. Due to the hysteretic behaviour is  
519 elastic, therefore, the two point was defined as  $(0.3\Delta_y, 0.3 F_y)$  and  $(-0.3 \Delta_y, -0.3 F_y)$ , respectively.

520 (2) Stiffness inflection points 2 and 6

521 Based on the investigation results in this study and reported by Zhao and Dun (2014), the inflection  
522 points of lateral stiffness of each of loops occur when the lateral displacement of the member reaches  
523 its corresponding yielding displacement level shown in Fig.12.

524 (3) End points 4 and 8 of initial unloading,  $F_{4,8}$

525 The initial unloading actions of SFSWs are stable (Lines 3-4 and 7-8) in the CSWs and will finish at a  
526 stable lateral force, as shown the lateral force at the points 4 and 8 in Fig.12. In this study, this stable  
527 lateral force is taken as 0.2 times yielding strength  $F_y$ .

528 5.2.3 Rules of hysteretic curve after maximum strength

529 Though the failure mode of all specimens is flexural-dominant failure, the skeleton curves of the  
530 CSW members after maximum strength is shorter than the one of individual shear walls or coupling  
531 beams. Therefore, the rules of the hysteretic curve after maximum strength are considered as same as  
532 that from yielding point to maximum strength point.

533 5.2.4 Stiffness of hysteretic model  $K_{23}$  and  $K_{67}$

534 Before the yielding of SFSW members, the stiffness of uploading is simplified as  $K_y$ . Based on the  
535 study, the various stiffnesses at post-yielding, i.e. the slop from yielding point to ultimate point, are  
536 obtained and shown in Fig.12.

537 **5.3 Verification of the proposed hysteretic model**

538 In order to confirm the proposed complete hysteretic model proposed, several representative loops of  
539 each specimen were used from the present study and the previous results (Meng 2013). These  
540 representative loops include the ones near to the cracking status, yielding status, maximum strength or  
541 ultimate strength status. Fig.13 shows the comparison results between experimental and predicated  
542 hysteretic loops which indicates that the proposed complete model assesses the hysteretic cycles of the  
543 RC/SFRC CSWs with a good agreement.

544

## 545 **6 Conclusions**

546 This paper experimentally investigated the hysteretic behaviour of SFRC CSWs under simulated  
547 seismic loads. The strength, deformation and stiffness degradation, energy dissipation and crack  
548 damage of the elements have been discussed. Main conclusions were drawn as follows.

549 (1) Steel fibres improve the stress distribution of RC CSWs in terms of lateral resistance capacity  
550 stiffness, and deformation. This is attributed to the fact that steel fibres improve the non-uniform  
551 situation of the stress of shear walls which makes the reinforcements provide more effective  
552 tensile resistance in the walls. Therefore, the deformation of entire CSW was realized by  
553 developing the flexural cracks at the ends of the shear walls and the shear-type cracks at the  
554 shear walls of the upper floors.

555 (2) Comparing with RC CSW specimens, SFRC CSWs presented a plump hysteretic behaviour with  
556 a higher lateral stiffness and strength, and more stable degradation of lateral resistance post-  
557 peak. Steel fibres delay the crack propagation of RC CSW specimens and the concrete crushing  
558 at the joint zone.

559 (3) Steel fibres improve the integrity of RC CSWs and the degradation of lateral stiffness of the  
560 members due to the tensile resistance of reinforcements in coupling beams is effectively used.  
561 This is because steel fibres improve the energy dissipation and deformation of coupling beam  
562 which was verified by the observed results of the reinforcement fracture in RC edge columns.



563 (4) Considering the coupling effectiveness of coupling beams, using a simplified strength model  
564 based on the sectional analysis of an individual shear wall, a maximum strength model has been  
565 developed for SFRC CSW specimens. Using the strength model, a simplified skeleton curve  
566 model and a hysteretic model were proposed for RC/SFRC CSWs. Results verified the proposed  
567 models can predict the experimental results and existing data with a good agreement.

568

569 **Acknowledgement**

570 The authors would like to thank the funding supports from National Natural Science Foundation No.  
571 51078333 and Program for Innovative Research Team in University (Sci.&Tech.) No.  
572 15IRTSTHN026.

574 **Notations**

575

$E_c J_{eq}$	—	equivalent stiffness, where $E_c$ is elasticity modulus of concrete;
$I_w$	—	moment of inertias of the entire cross-section of shear wall;
$A_w$	—	area of cross section of wall without openings reported by CIS (2002);
$\mu$	—	calculation factor of the shape of cross-section taken as 1.2 for the rectangular section;
$A_{sw}, A_s$	—	cross area of longitudinal steel rebars in the shear wall and edge columns;
$f_{yw}, f_y$	—	yielding strength of longitudinal steel in the shear wall and edge columns;
$x, x_t$	—	calculation height of compressive zone and tensile zone which is taken as $x_t = h_w - 1.25x$ ;
$h_w, h_{wo}$	—	height and effective height of cross section respectively;
$b_w, h_b, H$	—	the width of the cross-section, and height of columns and a total height of shear walls
$f_{fb}$	—	bending tensile strength of FRC, which can be calculated as $0.4f_{fs}$ ;
$f_{fc}, f_{fs}$	—	compression strength, splitting tensile strength of FRC obtained from test or the model proposed by Han et al. (2006) ;
$\Delta_y, \Delta_u$	—	yielding displacement ultimate displacement of the member when 85% $V_{max}$ ;
$\delta_u, \mu_{max}, \mu_u$	—	ultimate inter-storey drift ratio, the maximal and ultimate ductility of members;
$V_{max}, V_{imax}$	—	the maximum strength of member and the one at $i$ th cycle;
$\Delta_{max}, \Delta_{imax}, \Delta_x$	—	lateral displacement corresponding to $V_{max}$ and $V_{imax}$ , and the given $x$ displacement;
$E_T, E_i, E_N$	—	total, $i$ th cycle and normalized dissipated energy of RC member;
$I_{wo}, I_E, \nu_{eq}$	—	total work and energy indexes, and equivalent viscous damping coefficient of the member;
$K_{int}, K_y, K_{max}, K_u$	—	initial and yielding stiffnesses of the member; as well as lateral stiffness from yielding to maximum strength points, and the one after peak point;
$\alpha_l, \beta_y$	—	influencing factors for yielding strength and reduced stiffness;
$F_y, F_{max}, F_u, F_i$	—	forces corresponding to yielding, maximum and ultimate displacements in envelop curve model; as well as the forces at $i$ feature points of the skeleton curve model ( $i=1-8$ );
$M_w, M_{st}$	—	maximum moment capacity of member, and the moment provided by transverse steel;
$M_{st}, M_a, M_{FRC}$	—	the moment provided by longitudinal steel, axial load action, and fibre reinforced concrete;

576

577 **References**

578 Aksogan, O., Arslan, H. M., & Choo, B. S. (2003). Forced vibration analysis of stiffened coupled  
579 shear walls using continuous connection method. *Eng. Struct.*, 25(4), 499-506.

580 Aristizabal-Ocfaoa, J. (1987). Seismic Behavior of Slender Coupled Wall Systems." *J. Struct. Eng.*,  
581 113:10(2221), 2221-2234.

582 **Baczkowski, B. J. (2007). Steel fibre reinforced concrete coupling beams (Doctoral dissertation),**  
583 **Hong Kong University of Science and Technology.**

584 Barbachyn, S. M., Kurama, Y. C., McGinnis, M. J., & Sause, R. (2016). Testing and Behavior of a  
585 Coupled Shear Wall Structure with Partially Post-Tensioned Coupling Beams. *ACI Struct. J.*, 113(1),

586 111.

587 Bayrak, O., Sheikh, S. A. (1997). High-strength concrete columns under simulated earthquake  
588 loading. *ACI Struct. J.*, 94, 708-722.

589 Bharti, R., Chidambaram, R. S., & Kwatra, N. (2017). Influence of Fiber Reinforced Concrete on  
590 Plastic Behavior on Exterior Beam Column Joint under Cyclic Loading. *Procedia Engineering*, 173,  
591 1122-1129.

592 Borg, R. P., Baldacchino, O., & Ferrara, L. (2016). Early age performance and mechanical  
593 characteristics of recycled PET fibre reinforced concrete. *Construction and Building Materials*, 108,  
594 29-47.

595 Cai, G., Zhao, J., Degée, H., & Vandoren, B. (2016). Shear capacity of steel fibre reinforced concrete  
596 coupling beams using conventional reinforcements. *Engineering Structures*, 128, 428-440.

597 Canbolat, B. A., Parra-Montesinos, G. J., Wight, J. K. (2005). Experimental study on seismic  
598 behavior of high-performance fiber-reinforced cement composite coupling beams. *ACI Struct.*  
599 *J.*, 102(1), 159-166.

600 Chaallal, O. and Ghlamallah, N. (1996). Seismic Response of Flexibly Supported Coupled Shear  
601 Walls. *J. Struct. Eng.*, 122:10(1187), 1187-1197.

602 Chaallal, O., Thibodeau, S., Lescelleur, J., Malenfant, P. (1996b). Steel fiber or conventional  
603 reinforcement for concrete shear walls. *Concr. Int.*, 18 (6), 39-42.

604 Chaallal, O., Gauthier, D., and Malenfant, P. (1996a). Classification Methodology for Coupled Shear  
605 Walls. *J. Struct. Eng.*, 122:12(1453), 1453-1458.

606 Cheng, M. Y., Fikri, R., & Chen, C. C. (2015). Experimental study of reinforced concrete and hybrid  
607 coupled shear wall systems. *Eng. Struct.*, 82, 214-225.

608 China industry standards (CIS). (1996). *JGJ101-1996: Specification of test methods for earthquake*  
609 *resistant building*, Beijing.

610 Chinese association for engineering construction standardization (CEC). 2004. *CECS 38:2004,*  
611 *Technical Specification for Fiber Reinforced structures*, China Plan press, Beijing.

612 Chinese association for engineering construction standardization (CEC). 2009. *CECS 13-2009*,  
613 *Standard test methods for fiber reinforced concrete*, China Plan press, Beijing.

614 Chinese industry standards (CIS). (2010). *JGJ 3-2010: Technical Specification for Concrete*  
615 *Structures of Tall Buildings*, Beijing.

616 Deng, M.K., Liang, X.W., & Yang, K. (2008). Experimental Study on Seismic Behavior of High  
617 Performance Concrete Shear Wall with New Strategy of Transverse Confining Stirrups. In *The 14th*  
618 *World Conference on Earthquake Engineering*, October, pp.12-17.

619 Earthquake Engineering Research Institute [2010] EERI Special Earthquake Report-June 2010: *The*  
620 *Mw 8.8 Chile Earthquake of February 27, 2010*, Oakland, California.

621 Ehsani, M. and Wight, J. (1990). Confinement Steel Requirements for Connections in Ductile  
622 Frames. *J. Struct. Eng.*, 116:3(751), 751-767.

623 Farvashany, F. E., Foster, S. J., & Rangan, B. V. (2008). Strength and deformation of high-strength  
624 concrete shearwalls. *ACI structural journal*, 105(1), 21.

625 Ghee, A.B., Priestley, M.N., Paulay, T. (1989). Seismic shear strength of circular reinforced concrete  
626 columns. *ACI Struct. J.*, 86(1), 45-59.

627 Gong, B. and Shahrooz, B. (2001). Concrete-Steel Composite Coupling Beams. I: Component  
628 Testing. *J. Struct. Eng.*, 127:6(625), 625-631.

629 Gosain, N. K., Jirsa, J. O., & Brown, R. H. (1977). Shear requirements for load reversals on RC  
630 members. *J. Struct. Div.-ASCE*, 103(7), 1461-1476.

631 Gupta, A., & Rangan, B. V. (1998). High-strength concrete (HSC) structural walls. *ACI Structural*  
632 *Journal*, 95(2), 194-204.

633 Han, R., Zhao, SB., Qu FL. (2006). Experimental study on the tensile performance of steel fiber  
634 reinforced concrete. *China Civil Eng. J.*, 39(11), 63-67. (in Chinese)

635 Harries, K. A. (2001). Ductility and deformability of coupling beams in reinforced concrete coupled  
636 walls. *Earthq. Spectra*, 17(3), 457-478.

637 Harries, K. A., Gong, B., & Shahrooz, B. M. (2000). Behavior and design of reinforced concrete,  
638 steel, and steel-concrete coupling beams. *Earthq. Spectra*, 16(4), 775-799.

639 Harries, K., Mitchell, D., Cook, W., and Redwood, R. (1993). Seismic Response of Steel Beams  
640 Coupling Concrete Walls. *J. Struct. Eng.*, 119:12(3611), 3611-3629.

641 Hu, H. S., Nie, J. G., & Wang, Y. H. (2016). Shear capacity of concrete-filled steel plate composite  
642 coupling beams. *J. Constr. Steel Res.*, 118, 76-90.

643 Hwang, S. K., Yun, H. D., Park, W. S., Han, B. C. (2005). Seismic performance of high-strength  
644 concrete columns. *Mag. Concrete Res.*, 57(5), 247-260.

645 Jacobsen, Lydik S. (1960). Damping in composite structures. *P. 2nd World Conference of*  
646 *Earthquake Engineering.*. No2.1029-1044.

647 Jiang, H., Wang, B., & Lu, X. (2013). Experimental study on damage behavior of reinforced concrete  
648 shear walls subjected to cyclic loads. *Journal of earthquake engineering*, 17(7), 958-971.

649 Kabeyasawa, T., & Hiraishi, H. (1998). Tests and analyses of high-strength reinforced concrete shear  
650 walls in Japan. *ACI Special Publication*, 176, 281-310.

651 Kuang, J. S., Chau, C. K. (1999). Dynamic behaviour of stiffened coupled shear walls with flexible  
652 bases. *Comput. Struct.*, 73(1), 327-339.

653 Lequesne, R. D., Parra-Montesinos, G. J., & Wight, J. K. (2012). Seismic behavior and detailing of  
654 high-performance fiber-reinforced concrete coupling beams and coupled wall systems. *Journal of*  
655 *Structural Engineering*, 139(8), 1362-1370.

656 Lequesne, R., Setkit, M., Kopczyński, C., Ferzli, J., Cheng, M. Y., Parra-Montesinos, G., & Wight, J.  
657 K. (2011). Implementation of High-Performance Fiber Reinforced Concrete Coupling Beams in High-  
658 Rise Core-Wall Structures. *American Concrete Institute, ACI, Special Publication*, 280, 1-12.

659 Lu, X. and Chen, Y. (2005). Modeling of Coupled Shear Walls and Its Experimental Verification. *J.*  
660 *Struct. Eng.*, 131:1(75), 75-84.

661 Memon, M. S., & Sheikh, S. A. (2005). Seismic resistance of square concrete columns retrofitted with

662 glass fiber-reinforced polymer. *ACI Struct. J.*,102(5),774-783.

663 Meng Yao (2013). Seismic behavior of RC shear wall coupled by SFRC coupling beam. *Master*  
664 *thesis, No. 201012212313*, Zhengzhou Univ., 62pp.

665 Osorio, L. I., Paultre, P., Eid, R., & Proulx, J. (2014). Seismic behavior of synthetic fiber-reinforced  
666 circular columns. *ACI Struct. J.*, 111(1),189-200.

667 Pam, H. J., Kwan, A. K. H., & Islam, M. S. (2001). Flexural strength and ductility of reinforced  
668 normal-and high-strength concrete beams. *P. I. Civil ENG-STR B.*, 146(4), 381-389.

669 Park, W. S., & Yun, H. D. (2005). Seismic behaviour of steel coupling beams linking reinforced  
670 concrete shear walls. *Eng. Struct.*, 27(7), 1024-1039.

671 Park, W. S., & Yun, H. D. (2006). Seismic behaviour and design of steel coupling beams in a hybrid  
672 coupled shear wall systems. *Nucl. Eng.Des.*, 236(23), 2474-2484.

673 Parra-Montesinos, G. J. (2005). High-performance fiber-reinforced cement composites: an alternative  
674 for seismic design of structures. *ACI Struct. J.*, 102(5), 668-675.

675 Parra-Montesinos, G. J., Wight, J. K., Kopczyński, C., Lequesne, R. D., Setkit, M., Conforti, A., &  
676 Ferzli, J. (2017). Elimination of Diagonal Reinforcement in Earthquake-Resistant Coupling Beams  
677 through Use of Fiber-Reinforced Concrete. *ACI Special Publication*, 313, 1-8.

678 Paulay T., Priestley M.J.N. (1992) *Seismic design of reinforced concrete and masonry buildings*, John  
679 Wiley & Sons, INC.,768pp

680 Paulay, T. (1971). Coupling beams of reinforced concrete shear walls. *Journal of the Structural*  
681 *Division*, 97(3), 843-862.

682 Paulay, T., Binney, J. R. (1974). Diagonally reinforced coupling beams of shear walls. *ACI Special*  
683 *Publication*, 42, 579-598.

684 Singh, M. P., Singh, S. P., & Singh, A. P. (2014). Experimental study on the strength characteristics  
685 and water permeability of hybrid steel fibre reinforced concrete. *International scholarly research*  
686 *notices*, 2014.

687 Song, P. S., & Hwang, S. (2004). Mechanical properties of high-strength steel fiber-reinforced  
688 concrete. *Construction and Building Materials*, 18(9), 669-673.

689 Su, R. K. L., & Wong, S. M. (2007). Seismic behaviour of slender reinforced concrete shear walls  
690 under high axial load ratio. *Engineering Structures*, 29(8), 1957-1965.

691 Subedi, N. (1991). RC Coupled Shear Wall Structures. II: Ultimate Strength Calculations. *J. Struct.*  
692 *Eng.*, 117:3(681), 681-698.

693 Tejchman, J., & Kozicki, J. (2010). Experimental and theoretical investigations of steel-fibrous  
694 concrete (pp. 3-26). Berlin: Springer.

695 Yap, S. P., Alengaram, U. J., Jumaat, M. Z., & Khaw, K. R. (2016). Torsional and cracking  
696 characteristics of steel fiber-reinforced oil palm shell lightweight concrete. *Journal of Composite*  
697 *Materials*, 50(1), 115-128.

698 Yu, R., Spiesz, P., & Brouwers, H. J. H. (2014). Mix design and properties assessment of ultra-high  
699 performance fibre reinforced concrete (UHPFRC). *Cement and concrete research*, 56, 29-39.

700 Yun, H. D., Choi, C. S., & Lee, L. H. (2004). Behaviour of high-strength concrete flexural walls.  
701 *Proceedings of the Institution of Civil Engineers-Structures and Buildings*, 157(2), 137-148.

702 Zhang HZ., Zhang RJ., Huang CK. (2007). Experimental study of shear resistance of steel fiber  
703 reinforced high strength concrete coupling beams. *China Civil Eng. J.*, 40(11),15-22. (in Chinese)

704 Zhang, M. (2007). Experimental research on flexural and seismic behavior of steel fiber reinforced  
705 concrete shear wall. *Master thesis, No. 04301409*, Zhengzhou Univ., 86pp. (in Chinese)

706 Zhang, Y., & Wang, Z. (2000). Seismic behavior of reinforced concrete shear walls subjected to high  
707 axial loading. *Structural Journal*, 97(5), 739-750.

708 Zhao, J., Dun, H. (2014). A restoring force model for steel fiber reinforced concrete shear walls. *Eng.*  
709 *Struct.*, 75, 469-476.

711 **Figures and tables in the study**

712

713 Fig.1 Coupled shear wall system: seismic effect and design

714 Fig.2 Details of the dimensions of test specimens

715 Fig.3 Experimental setup

716 Fig.4 Hysteretic behaviour of the tested CSW specimens

717 Fig.5 Crack situation of the specimens SFSWs 1-3 (at the end of testing, after  $4\Delta y$ )

718 Fig.6 Strain-displacement of longitudinal reinforcements of shear walls

719 Fig.7 Main assessment factors of RC members under seismic loads

720 Fig.8 Degradation of lateral secant stiffness of CSWs with displacement

721 Fig.9 Typical skeleton models of RC/FRC members

722 Fig.10 Comparison between proposed model and experimental skeleton curves

723 Fig.11 Main characteristics of the hysteretic curve of SFRC CSWs

724 Fig.12 Proposed hysteretic model of RC/SFRC CSWs

725 Fig.13 Comparison between experimental and predicted hysteretic cycles

726

727 Table.1 Details of main parameters of specimens

728 Table.2 Summary for the test results of CSWs in this study

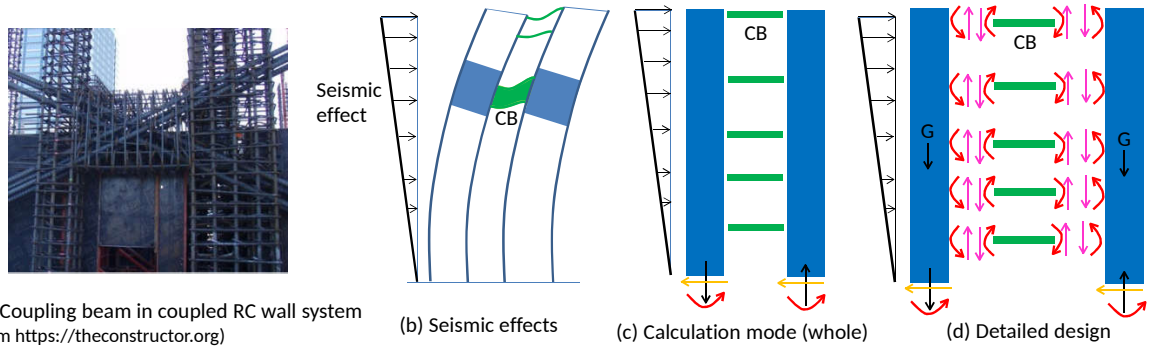
729

730

731

732

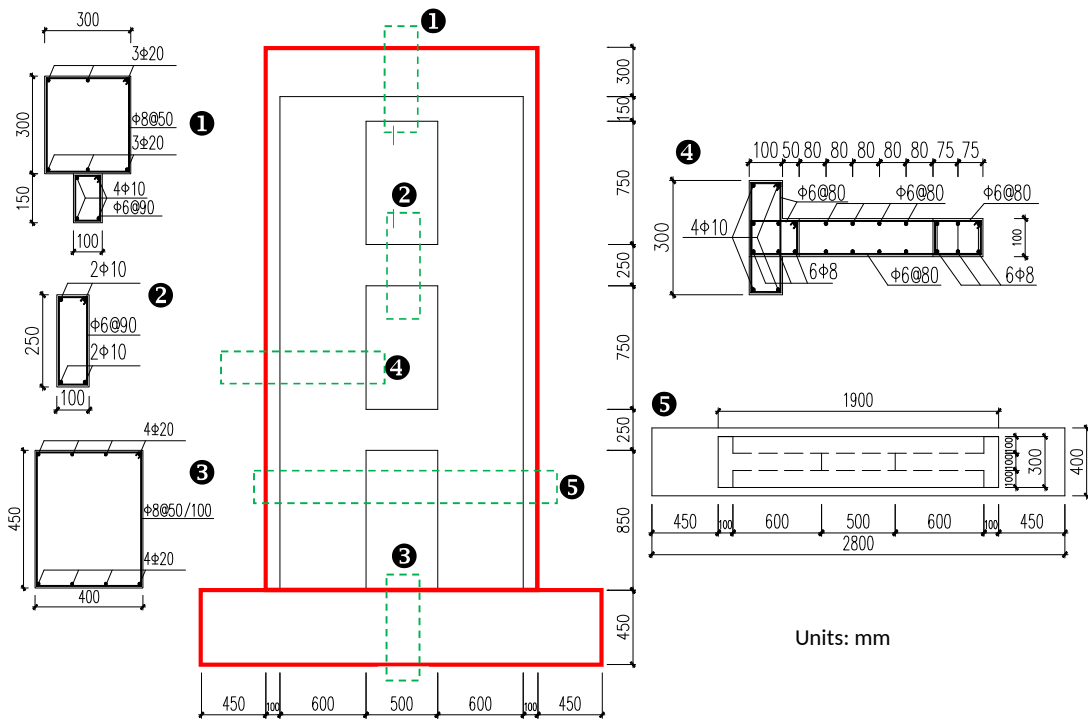




734

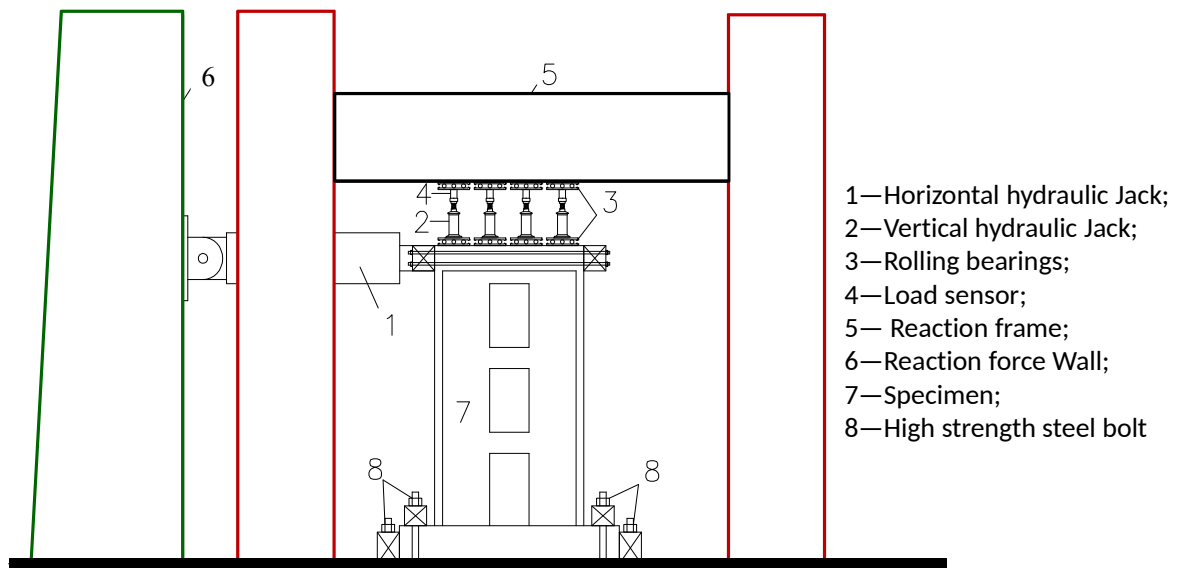
735 Fig.1 Coupled shear wall system: seismic effect and design

736



737

738 Fig.2 Details of the dimensions of test specimens



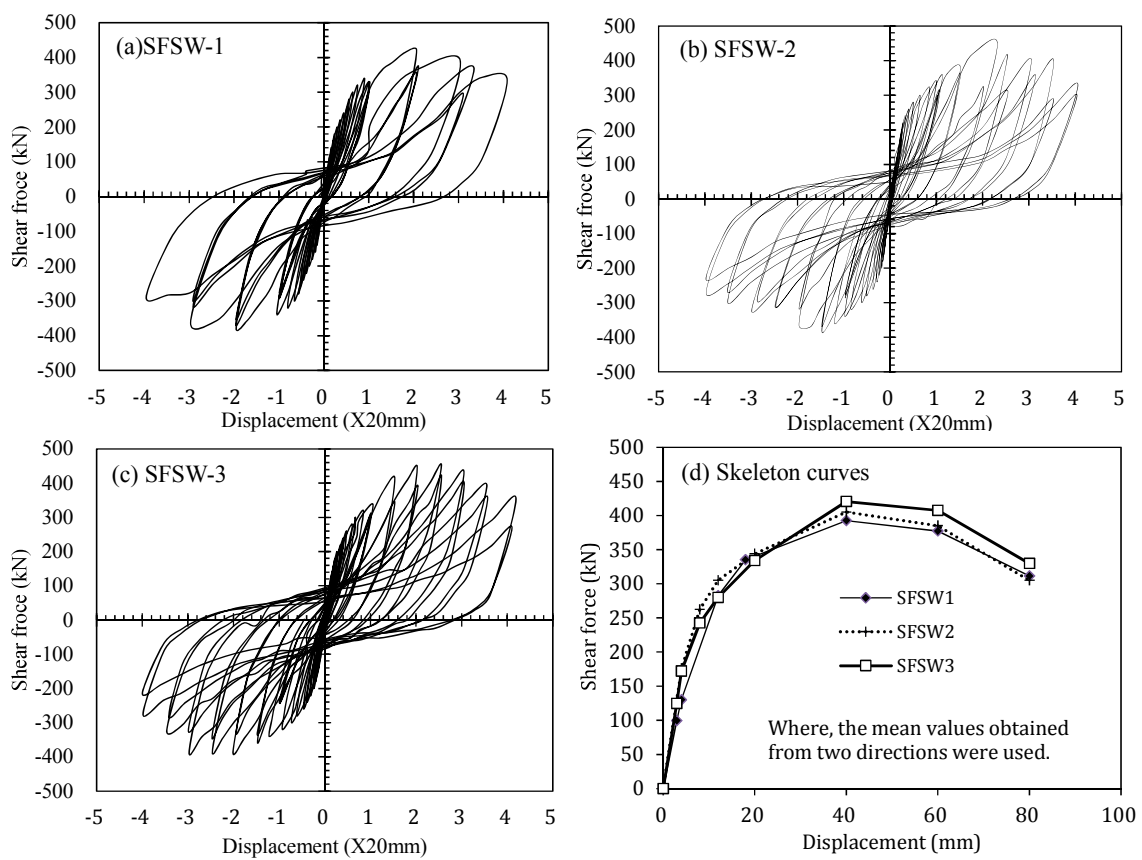
739

740 Fig.3 Experimental setup

741

742

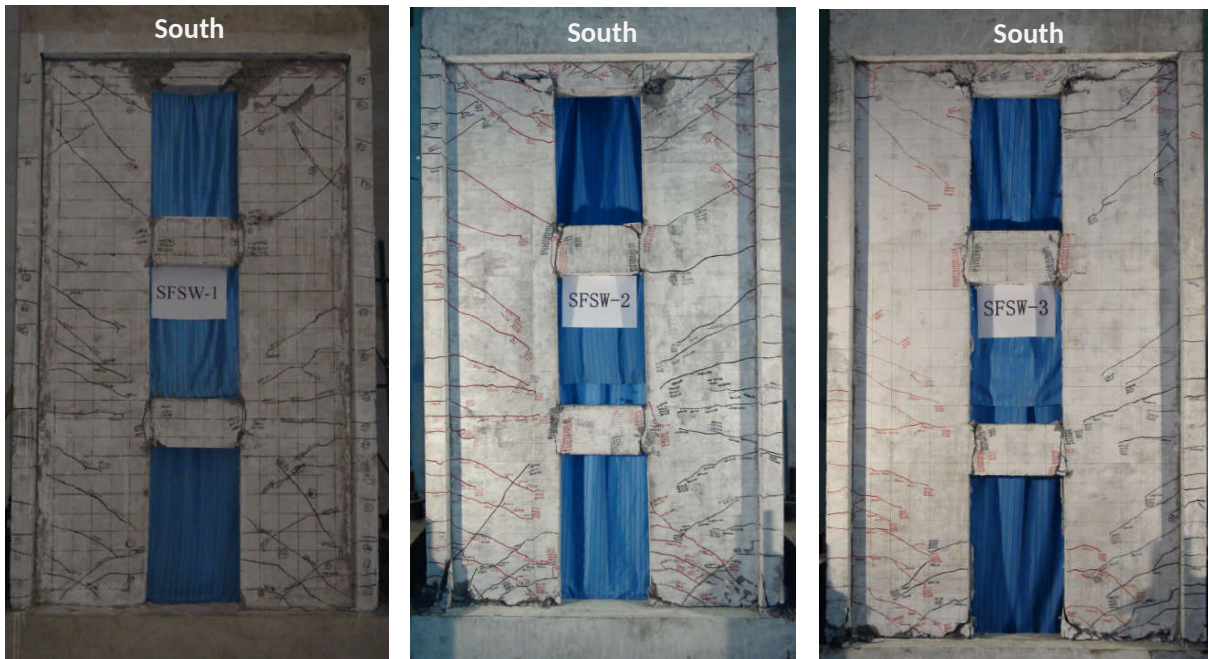
743



744

745 Fig.4 Hysteretic behaviour of the tested CSW specimens

746

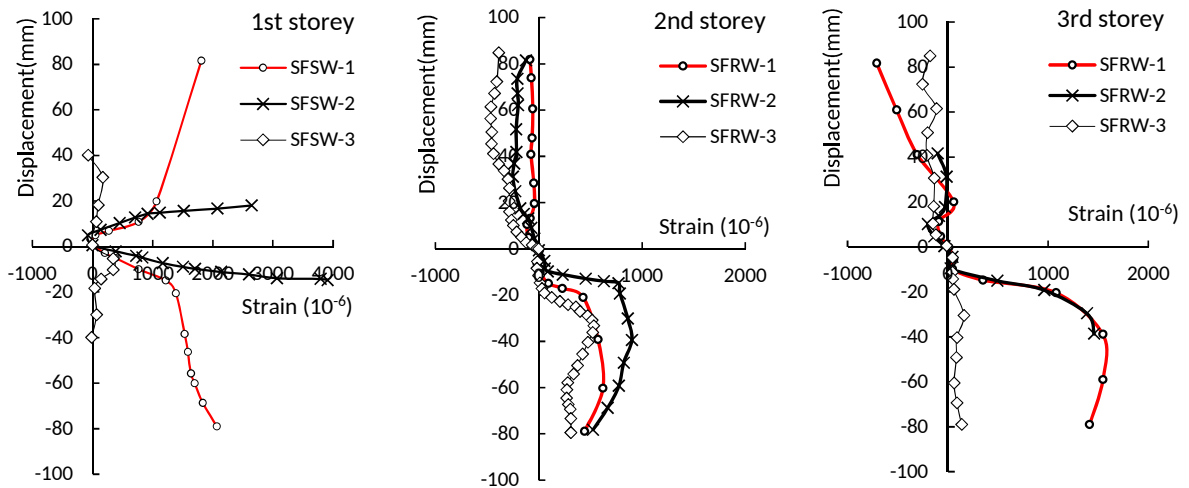


747

748

749

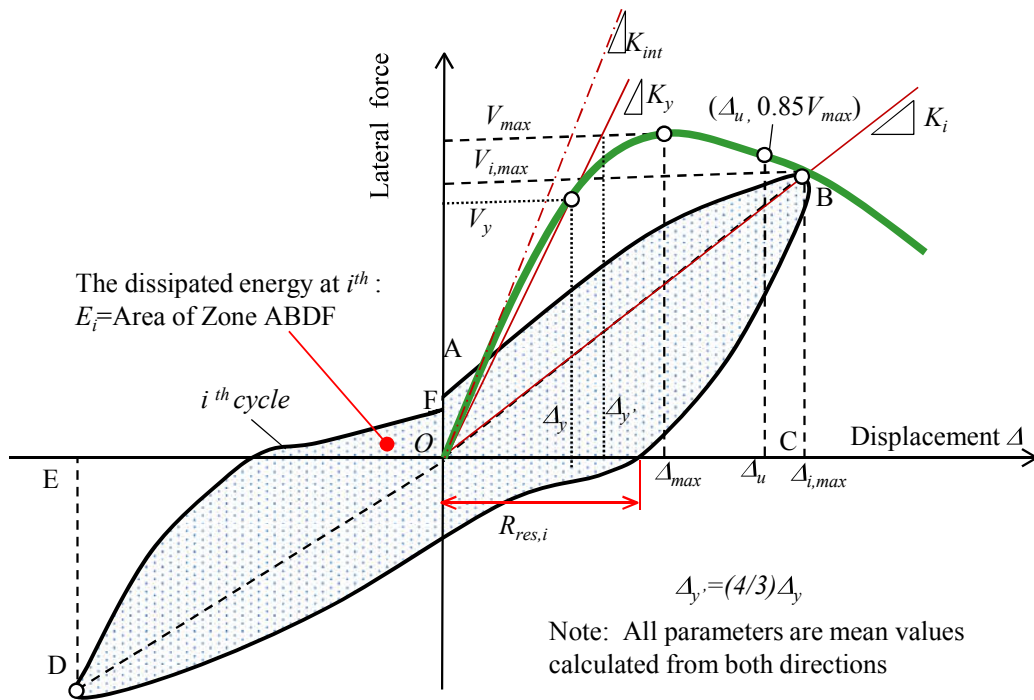
Fig.5 Crack situation of the specimens SFSWs 1-3 (at the end of testing, after 44y)



751

752 Fig.6 Strain-displacement of longitudinal reinforcements of shear walls

753



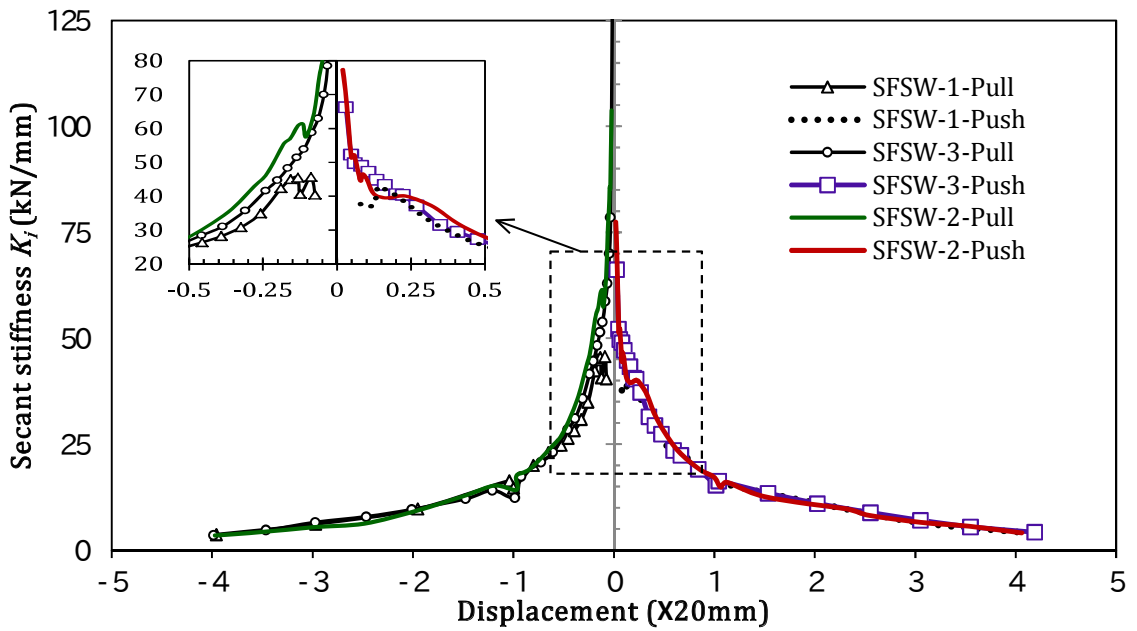
754

755 Fig.7 Main assessment factors of RC members under seismic loads

756

758

759

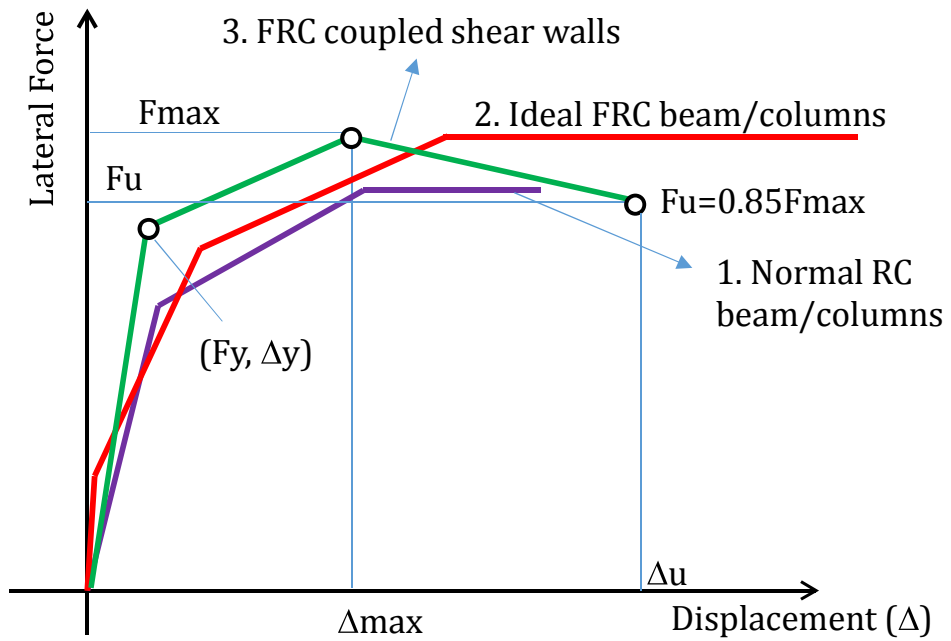


760

761

Fig.8 Degradation of lateral secant stiffness of CSWs with displacement

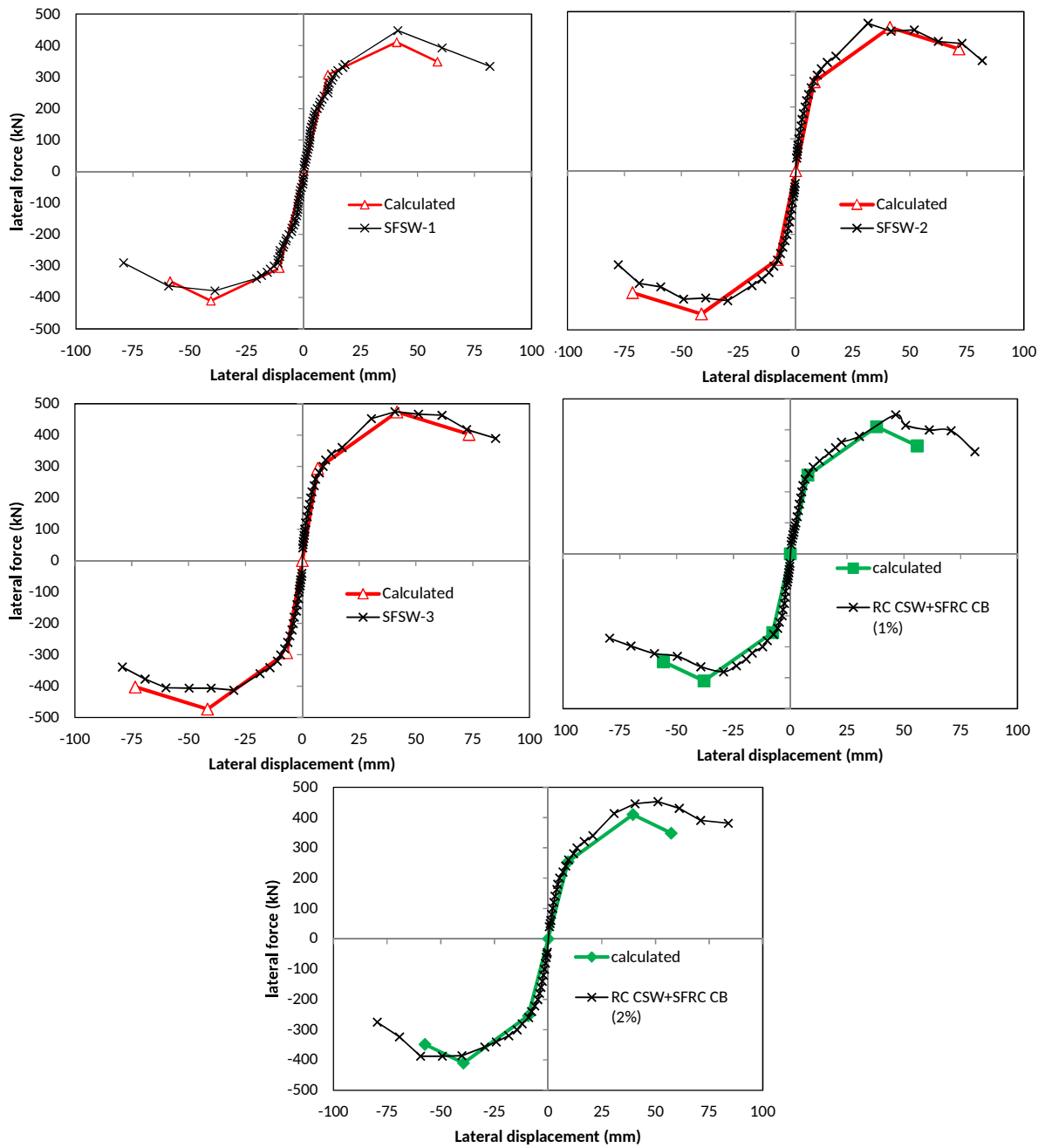
762



763

764

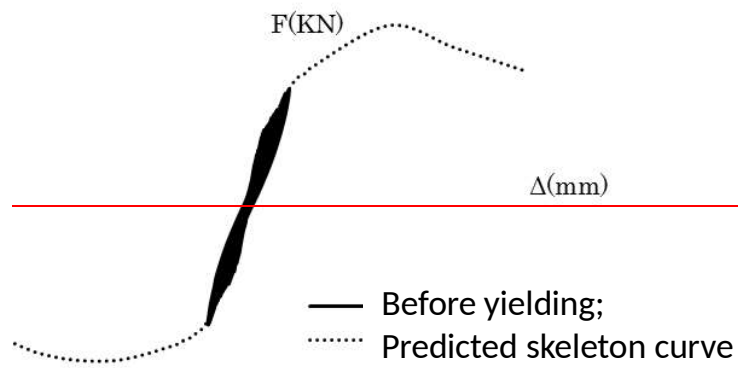
Fig.9 Typical skeleton models of RC/FRC members



765

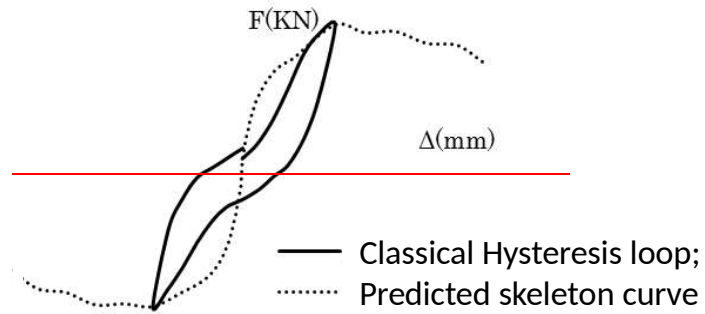
766 Fig.10 Comparison between proposed model and experimental skeleton curves

767



(a) Before yielding strength of elements

768

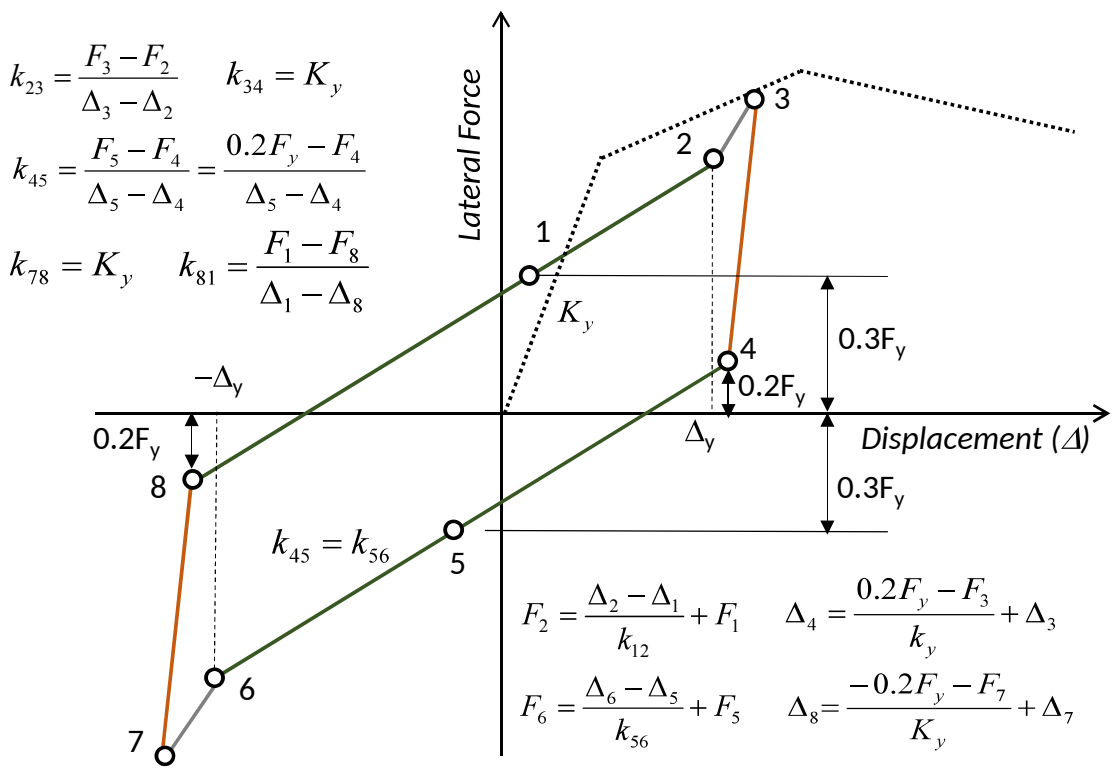


(b) Before ultimate strength of elements

769

770 Fig.11 Main characteristics of the hysteretic curve of SFRC CSWs

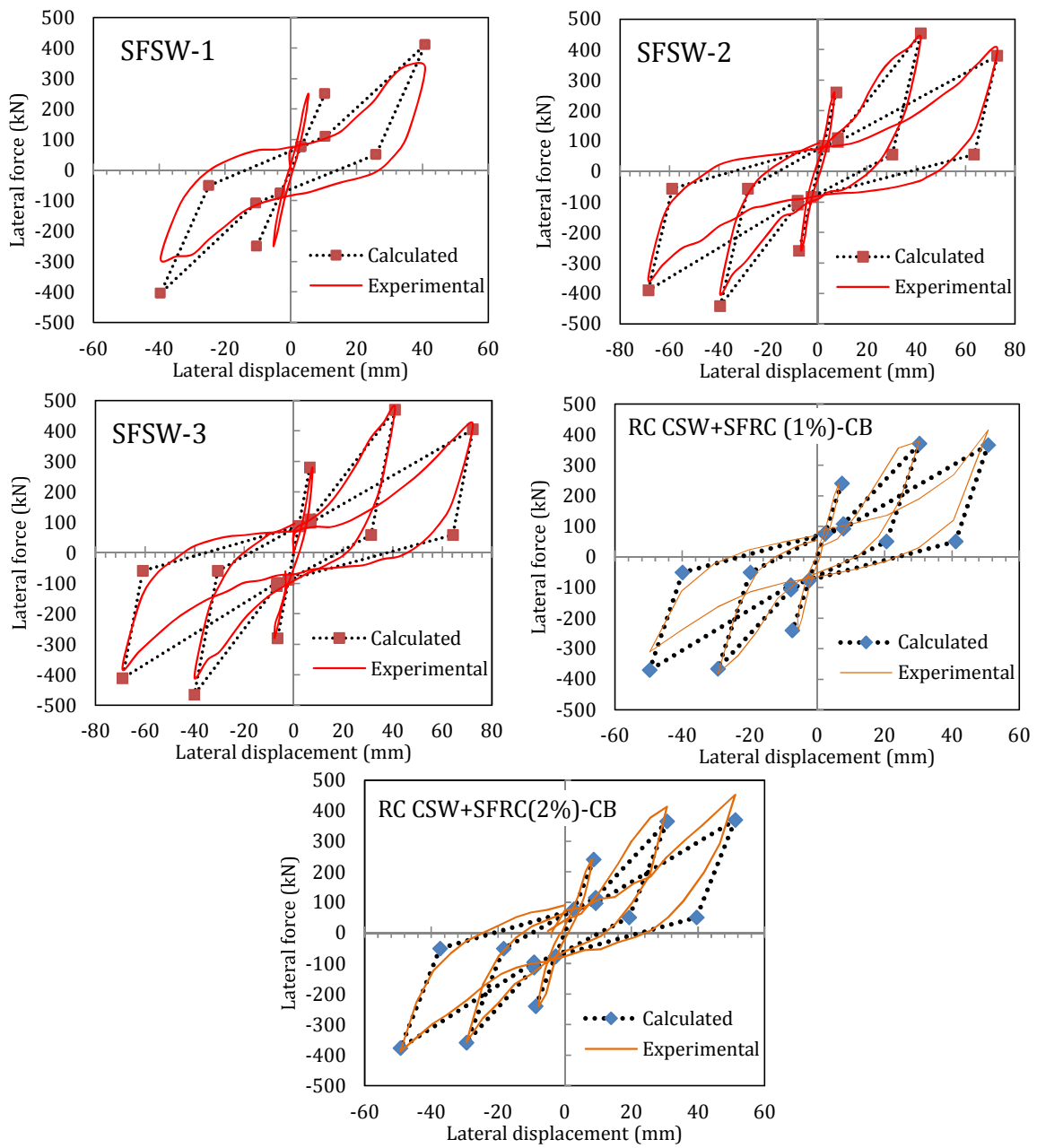
771



772

773 Fig.12 Proposed hysteretic model of RC/SFRC CSWs





774

775 Fig.13 Comparison between experimental and predicted hysteretic cycles

777 Table.1 Details of main parameters of specimens

Specimen No.	Coupling beam Length/width/height (mm)	SFRC		Steel fibre			
		$f_{fc}$ (MPa)	$f_{fts}$ (MPa)	Volume fraction	Yielding strength (MPa)	Diameter (mm)	Length/Diameter
SFSW-1		41.7	3.17	0			
SFSW-2	500/100/250	46.44	3.85	1%	380	0.76	42
SFSW-3		50.37	4.29	2%			

778 SFRC: Steel fibre reinforced concrete;  $f_{fc}$ : SFRC compressive strength;  $f_{fts}$ : Splitting tensile strength.

779

780

781 Table.2 Summary for the test results of CSWs in this study

Specimens	$V_{max}$ (kN)	$K_{int}$ (kN/mm)	$K_y$ (kN/mm)	$\Delta_y$ (mm)	$\mu_{max}$	$\mu_u$	$\delta_u$ (%)	$E_T$ (kN.mm)	$E_N$	$I_{wo}$	$I_E$
SFSW-1	401.30	36.79	20.67	20.00	1.51	2.54	2.15	134181.06	16.23	24.17	22.60
SFSW-2	414.76	51.35	20.74	20.00	1.61	2.26	1.91	203410.94	24.52	38.18	31.88
SFSW-3	420.15	52.20	21.01	20.00	2.07	2.65	2.25	220256.12	26.21	36.44	31.93

782

783

784

785